J MATER RES TECHNOL. 2014;3(2):179–185

Available online at www.sciencedirect.com

jmr&t Journal of Materials Research and Technology

www.jmrt.com.br

Review Article

Absorption of non-metallic inclusions by steelmaking slags—a review

Bruno Henrique Reis, Wagner Viana Bielefeldt, Antônio Cezar Faria Vilela*

Universidade Federal do Rio Grande do Sul, Porto Alegre, RS, Brazil

ARTICLE INFO

Article history:
Received 4 February 2014
Accepted 15 March 2014
Available online 14 April 2014

Keywords:
Steel
Cleanliness
Inclusions
Slag
Absorption
Removal
Flotation
Separation
Dissolution

ABSTRACT

The formation of non-metallic inclusions during steelmaking is inevitable and, when not properly controlled, can cause performance and production problems. Slag is one of the resources available to carry out this control. In steelmaking, it is generally understood that inclusions are naturally absorbed by slag when flotation is sufficient. However, separation and dissolution may define the inclusion absorption capacity of slag. The discussion in this review explains the relationship between separation and the contact angle at the steel/inclusion interface, which differentiates the mechanism from liquid and solid inclusions. Whereas liquid particles show more predictable behavior in experimental observations, thermodynamic analysis is necessary in order to describe the removal of solid particles. Among other findings, it is evident that slag viscosity and the formation of compounds at the inclusion/slag interface strongly influence inclusion dissolution capacity. Following a detailed description of findings in the literature, this review considers the most influential factors to aid in optimizing slags for inclusion absorption.

1. Introduction

Controlling non-metallic inclusions is essential in the production of clean or high purity steel. An excessive number of inclusions or inadequate morphology can lead to problems such as: *clogging*, breaking of the wire rod during drawing, hydrogen induced cracking (HIC), embrittlement at low temperatures, fatigue failure and surface quality degradation, among others. Inclusions are formed by oxidation, producing endogenous inclusions, or via reoxidation, refractory breakage and slag emulsification generating exogenous inclusions. In addition, temperature differences can modify the solubility limit of steel, causing inclusions in the event of cooling or solidification, for example [1,2].

In this respect, studying the inclusion absorption capacity of slag is promising. The removal of non-metallic particles occurs in three stages: flotation, separation and dissolution. However, the controlling steps, most influential factors and the different ways to optimize this process can only be

* *Corresponding author.*
E-mail: wagner@ct.ufrgs.br (W.V. Bielefeldt).
http://dx.doi.org/10.1016/j.jmrt.2014.03.011

determined by observing these phenomena in real time. As such, several studies have been carried out to clarify inclusion/slag interaction, particularly over the last decade, with the advent of Confocal Scanning Laser Microscope (CSLM) technology. This equipment allows adequate visualization of inclusion absorption by slag at steelmaking temperatures. Combined with chemical and physical characterization techniques for steel, slag and inclusions, it provides a range of studies that this review aims to clarify.

2. Inclusions absorption by slag

Most authors report that inclusion absorption by slag occurs in three stages [2–5]:

(i) Flotation in the bath – transport of the inclusion to the steel/slag interface.
(ii) Separation of liquid steel – movement of the inclusion to the interface, breaking the surface tension of steel.
(iii) Dissolution in slag – removal of the inclusion from the steel/slag interface for full incorporation into the slag.

An inclusion can only be considered eliminated from steel when it is completely dissolved in the slag. Most research based on fluid dynamics that seeks to optimize inclusion arrival at the steel/slag interface assumes that, once there, the inclusion is removed from the steel. However, for this to occur, the inclusion must first separate from the steel to the interface and then from the interface to the slag. These steps correspond to separation and dissolution, respectively. Should this not occur, the inclusion will be able to return to the steel bath, depending on the flow patterns in the ladle or tundish [4–7]. Thus, in order to obtain clean steel, the slag must satisfy two basic requirements: it must exhibit substantial wettability with inclusions and provide high inclusion dissolution rates [8].

3. Stage I – flotation

To date, flotation is the most widely studied of the three inclusion removal stages. Using physical and computer simulations, researchers seek to identify optimum flow models for the removal of particles similar to inclusions.

Fruehan [9] refers to studies where inclusion flotation was modeled using a particle coalescence theory and an algorithm capable of describing turbulent flow with recirculation. There is also reference to a study that established a simple equation for inclusion flotation as a function of rinsing time. Rinsing was performed using specific valves and the equation is only valid under these conditions. Nevertheless, there is no doubt that agitation of the bath by gas injection contributes to transporting the inclusions to the metal/slag interface.

In a literature review, Daoud [10] shows that the flow of the liquid phase in steel reservoirs is governed by equations for the conservation of momentum (Navier–Stokes) and mass (continuity). Several approaches can then be adopted and research differs as to the computational models applied. Daoud [10] also analyzed previous research that uses computer simulation of the fluid dynamics in a tundish. The author found that most studies adopt the $k-\varepsilon$ turbulence model when simulating the flow of steel, and the Lagrangian model for particle motion. He also reports that, during continuous casting, only some of the particles are removed by flotation in the tundish. These particles are lighter than steel and therefore reach the slag layer through buoyancy force. Rising velocity depends on the diameter, shape and specific mass of the inclusion; smaller particles have slower rising velocity and are difficult to remove via flotation, whereas larger particles are more easily removed.

It is important to note that, near the metal/slag interface, steel tends to flow parallel to the interface and inclusions, particularly small ones, tend to follow the flow of steel. Therefore, in order to efficiently remove inclusions, they must bind securely to the slag on reaching the interface. This promotes rapid dissolution and prevents the particles, which tend to follow the flow of steel, from returning to the steel bath [8].

4. Stage II – separation

Thermodynamics shows that all inclusions exhibit lower energy when separated from liquid steel to a liquid steel/slag, liquid steel/gas or liquid steel/refractory interface. However, for this to occur, the liquid steel between the inclusion and the interface must be drained, allowing a hole to form between the two interfaces. Once the hole has formed, it uses interfacial energy to grow spontaneously and the inclusion is absorbed by the steel/slag interface. This step requires that inclusion energy exceed the interfacial energy that separates the two liquids. When there is insufficient energy, the particles (solid inclusions) or droplets (liquid inclusions) stabilize for long periods, called rest times, which precede separation. In a dynamic system, particles or droplets may be re-entrained into the steel during the rest time. As such, these inclusions display poor removal efficiency and agglomeration is necessary to increase their size. This increase ensures greater buoyancy and inertia force, enabling inclusions to overcome interfacial forces and ensure complete separation [5].

Milmann [11] differentiates the behavior of solid and liquid inclusions in the separation phenomenon as a function of the contact angle. Solid inclusions have a large contact angle at the steel/inclusion interface. Thus, on nearing the steel/slag interface, substantial driving force allows these inclusions to separate from the steel and prevents re-entrainment. For liquid inclusions, however, this mechanism is hampered due to the low contact angle between these inclusions and the steel. This maintains the film of liquid steel stable as the inclusions approach the steel/slag interface. For liquid inclusions, the fracture and drainage kinetics of the steel film is hindered, making the separation process less favorable than for solid inclusions.

The contact angle determines the wettability between the inclusion and steel or the inclusion and slag. Thus, slags with greater wettability than inclusions are more likely to separate these inclusions from steel. In this context, Choi and Lee [8] placed several liquid slags from the $CaO–Al_2O_3–SiO_2$ system in contact with a solid Al_2O_3 substrate. The experiments made it possible to determine the contact angle between these slags and the substrate, as well as the influential factors. For

example, the authors found that the contact angle is higher for slags with greater surface tension, but viscosity variations do not cause a significant change in the angle. Changes in basicity and alumina content demonstrate a significant impact. Slags with greater basicity and/or lower alumina content exhibit a larger contact angle with the substrate. These slags therefore have greater wettability over the solid. These findings demonstrate how slag properties can influence the separation phenomenon.

In an analysis of solid inclusions, Valdez, Shannon and Sridhar [13] adapted the hydrodynamics-based model proposed by Bouris and Bergeles [12] to study the forces involved in the separation phase. This approach considers the inclusion as a rigid and inert sphere, reaching a flat and static steel/slag interface that is free of turbulence. Moreover, the model assumes that the particle is small enough not to alter the steel/slag interfacial tension as it moves from the steel to the interface. Thus, inclusion motion is governed by the balance between four forces: capillary force, buoyancy force, friction force and added mass force. One of the parameters that govern these forces is the Reynolds number (Re), which generates two possible situations. For $Re > 1$, the particle is covered by a film of liquid steel that prevents direct contact with the slag. By contrast, if $Re < 1$, the particle reaches the interface at low enough velocity to allow for flow of the film and direct contact with the slag. Moreover, if $Re < 1$, the slag acts on the particle and generates a rebound force that also forms part of the system's set of vectors. Based on the balance between these forces, Valdez, Shannon and Sridhar [3] tested normal and extreme values for the following variables: interfacial tension between slag and the inclusion (σ_{IS}), particle diameter, particle velocity on reaching the steel/slag interface and slag viscosity. In cases where 100% separation took place, the time predicted by the model for separation to occur was considered insignificant, since less than 7E-4 [s] was calculated for the slowest situation. Only when the extreme value of 0.6 [N/m] was simulated for σ_{IS} (the normal value varies between 0.01 and 0.2 [N/m]), did incomplete separation occur (approximately 90%), which implies infinite time for this stage.

Lee et al. [7] experimentally analyzed separation times using the CSLM technique (Confocal Scanning Laser Microscope), with slag containing 50% CaO and 50% Al_2O_3 (for mass percentages). Solid inclusions separation occurred so quickly that the instruments used were unable to determine a process time. The authors could only establish that alumina inclusions rested and agglomerated on the interface, even against the direction of fluid flow. They also analyzed separation for liquid inclusions, identifying times between 2 and 7 s for the particle (from its arrival at the interface) to be completely incorporated by the slag. However, some of the liquid inclusions did not pass through the interface and were re-emulsified. These results are in agreement with Milmann's theorem [11] when analyzing the contact angle, as previously mentioned.

The separation of inclusions to the steel/refractory interface can be dangerous, since it may serve as a nucleus for the growth of inclusion agglomerations. As observed in the clogging phenomenon, these clusters can break and be dragged back into the steel. Controlling the turbulence of steel flow is therefore essential [5]. This also emphasizes the importance of optimizing dissolution in order to shorten the length of time in which inclusions are susceptible to agglomeration.

5. Stage III – dissolution

Dissolution is not problematic for liquid solutions since these are predominantly miscible in the ladle, tundish or mold slags covering them [5]. This affirmation is in accordance with the observations of Lee et al. [7]. Their study reported that liquid inclusions dissolved immediately on contact with the slag analyzed. However, no other studies were found that described the dissolution mechanism of liquid inclusions.

By contrast, solid inclusions have limited solubility in slags and are therefore sensitive to the physical and chemical characteristics, temperature gradients and volume of the slag in question [5,6,8,13]. As a result, the dissolution of solid inclusions is controlled by mass transfer and may be limited by diffusion or reaction kinetics. Additionally, the efficiency of this mechanism may be impaired by chemical reactions with the slag [2,3,5,6,13].

5.1. *Mass transfer control*

Choi et al. [6] conducted an experiment with an alumina cylinder rotating inside a liquid slag. Although this situation is unlikely in industrial practice, the authors were able to observe the direct relationship between the decline in the cylinder's radius and the rotation speed. They found that the dissolution of alumina is at least partially controlled by mass transfer in slag with CaO and Al_2O_3 content above 38% (for mass percentages), with the remaining percentage corresponding to SiO_2. This observation contributed toward formulating Eq. (1), which determines the dissolution rate of alumina.

$$-\frac{dr}{dt} = k\left(\frac{\rho_{slag}}{100 \cdot \rho_{Al_2O_3}}\right)[mass\%\,Al_2O_{3s} - mass\%\,Al_2O_{3b}] \quad (1)$$

The terms of Eq. (1) are: dissolution rate (dr/dt); mass transfer coefficient (k); slag density (ρ_{slag}); alumina density (ρAl_2O_3); mass percentage of alumina in the interface ($mass\%\ Al_2O_{3s}$); mass percentage of alumina in the slag ($mass\%\ Al_2O_{3b}$).

Eq. (1) provides the driving force for the dissolution phenomenon expressed as the difference in alumina content from the interface to the slag. It can be noted that the higher this value, the greater the magnitude of the dissolution rate.

Valdez, Shannon and Sridhar [3] used the Shrinking Core Model [14] as a basis in proposing Eq. (2), when dissolution is controlled by diffusion.

$$\tau = \frac{\rho \cdot Ro^2}{2 \cdot D \cdot [C_{(p)} - C_{(s)}]} \quad (2)$$

The terms of Eq. (2) are: total dissolution time of the inclusion (τ); inclusion density (ρ); initial radius of the inclusion (Ro); diffusion coefficient of the species with the slowest diffusion (D); difference in particle concentration at the interface (p) and in the slag (s), ($C_{(p)} - C_{(s)}$, which can be simplified to ΔC). Eq. (2) shows the same influence of the driving force, ΔC, established

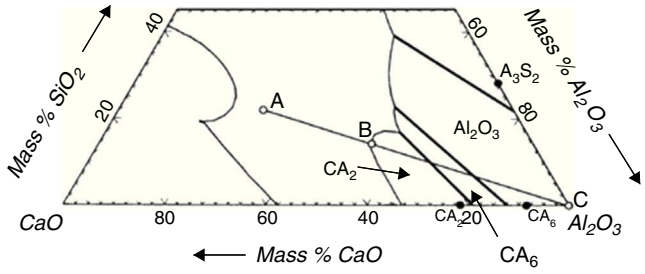

Fig. 1 – Ternary diagram for $CaO–SiO_2–Al_2O_3$ showing a graphic example of driving force, ΔC (segment BA), and the dissolution pathway for alumina to slag A (segment CA). Adapted from Ref. [6].

in Eq. (1). In this case, as the ΔC increases, the time needed for dissolution decreases, that is, the dissolution rate rises.

Valdez, Shannon and Sridhar [3] also report that when dissolution is not controlled by diffusions, it is because the dissolution reaction is slow. In other words, there is no saturation of inclusion components in the slag. Thus, the process is controlled by the reaction kinetics on the surface of the solid particle. The formula that describes this process, in Eq. (3), is adjusted in accordance with the Shrinking Core Model.

$$\tau = \frac{\rho \cdot Ro}{kr[C_{(p)} - C_{(s)}]} \quad (3)$$

The variables in Eq. (3) are the same as those in Eq. (2), with the exception of k_I, which represents the constant dissolution reaction rate. For this case, the driving force for dissolution appears in the form of inclusion concentration at the interface and in the slag ($C_{(p)} - C_{(s)}$). A graphic example of ΔC can be seen in Fig. 1.

5.2. *Chemical reactions at the interface*

The driving force for inclusion dissolution alone, as defined by the ternary diagram in Fig. 1, does not allow for the effect of chemical reactions on the dissolution rate, for example. As such, several authors experimentally investigated the velocity of dissolution reactions to determine the influence of other factors [2,3,5,6,13].

5.2.1. *Al_2O_3 inclusions*

Choi et al. [6] put liquid slags of CaO, SiO_2 and Al_2O_3 into contact with solid sintered alumina. Several samples were quickly removed from the heating zone and cooled with helium gas to determine the predicted reactions. The result obtained by SEM/EPMA (scanning electron microscope/electron probe micro-analyzer) confirmed the formation of $CaO{\cdot}2Al_2O_3$ (CA_2) and $CaO{\cdot}6Al_2O_3$ (CA_6), identified as possible intermediate compounds by the diagram in Fig. 1. Thus, should a liquid slag have a composition close to that at point A in Fig. 1, these calcium-aluminates may be formed. Linearity in the reaction pathway is expected, given that the proportion between calcium oxide and silica is kept constant. However, the stability of these compounds depends on dissolution kinetics.

Table 1 – Slags from the experiments by Park et al. [2] (in wt%).

	M1	M2				M3
		M21	M22	M23	M24	
CaO	43.3	48.7	43.5	38.4	33.2	53.4
Al_2O_3	4.97	4.99	14.9	24.9	34.9	4.97
SiO_2	51.3	46.3	41.5	36.7	31.8	41.6
CaO/SiO_2	0.85	1.05	1.05	1.05	1.05	1.28

Park et al. [2] conducted experiments using the same system as Choi et al. [6], but with different slag compositions, as per Table 1.

The methodological differences between the two studies do not compromise the comparisons made below. The results were similar to those of Choi et al. [6]. However, in addition to analyzing the products, Park et al. [2] plotted the compositions found during dissolution on a ternary diagram (Fig. 2).

On observing the evolution of compositions at the inclusion/slag interface, particularly for the slags M21, M22 and M3, it can be noted that the linearity reported by Choi et al. [6] does not always occur. The deviation observed for the inclusions in this system changed the reaction pathways to the extent of forming unexpected compounds purely by thermodynamic analysis.

In addition, Park et al. [2] identified the structures formed by the compounds through images, using the CSLM technique. For M1, CA_6 formed on the surface of Al_2O_3 particles, maintaining the surface smooth throughout dissolution. For M21, M22, M23 and M24, the products were CA_6 (external), which also maintained the surface smooth during dissolution, and CA_2 (internal). These layers were also found to be closely joined by needle-like structures. M3 showed a complex order of layers, where the surface became uneven during dissolution. The products of M3 were CA_6, CA_2 and $Ca_2Al_2SiO_7$ in the inner layer and $Ca_2Al_2SiO_7$, with a dense appearance, in the

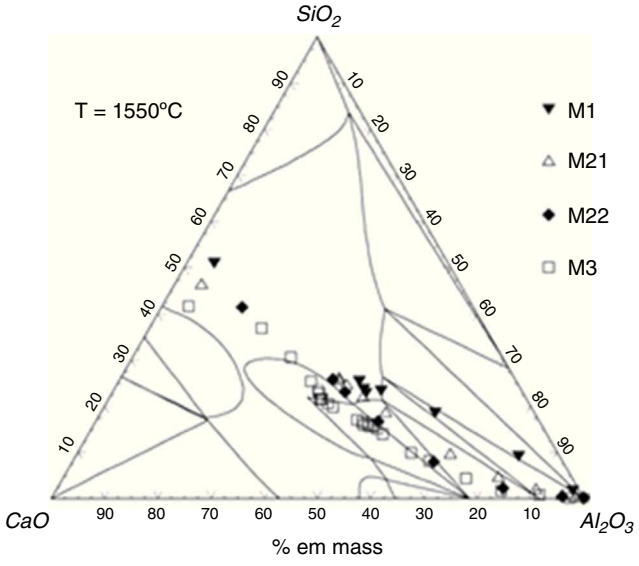

Fig. 2 – Dissolution pathways for Al_2O_3 in $CaO–SiO_2–Al_2O_3$ slags [2].

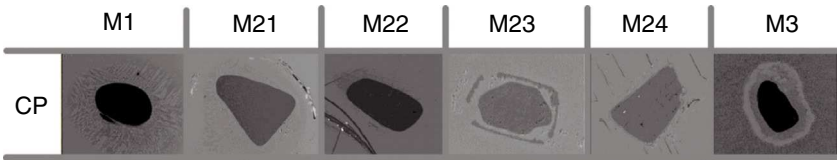

Fig. 3 – Image obtained by SEM of the MgO inclusion in 6 different slags. Adapted from Ref. [2].

outer layer. Liquid phase formation in the irregularities of the structure of M3 was questioned, but could not be proven.

On the other hand, Valdez et al. [15] observed that alumina maintained a smooth surface during dissolution when in contact with CAS slag (36% CaO, 21% Al_2O_3, 42% SiO_2 and 0.4% MgO, for mass percentages), but analysis by SEM/EDS identified no products. Nevertheless, the surface was thick when in contact with CASM slag (39.5% SiO_2, 33.4% CaO, 19.5% Al_2O_3 and 7.3% MgO, for mass percentages) and SEM/EDS analysis identified the presence of spinel ($MgAl_2O_4$) at the interface. Spinel formation on the surface of sintered steel (dissolved in slag $CaO/SiO_2 = 0.8$, containing 9% Al_2O_3 and 5–15% MgO) was also described by Taira, Nakashima and Mori [17]. The authors found that reduced dissolution speed as a function of greater MgO content in the slag was the result of suppressed flow of the slag components through the spinel layer.

5.2.2. *MgO inclusions*

Valdez et al. [13] studied the dissolution of MgO inclusions in slags of the CaO–SiO_2–Al_2O_3 system composed of 42% silica, 36% lime, 21% aluminum and 0.4% magnesium. The results obtained by SEM/EDS showed that the products in the reaction layer were pure spinel ($MgAl_2O_4$).

Park et al. [2] did the same for the slags shown in Table 1. The approach was slightly different to alumina analysis, since the CaO–MgO–Al_2O_3–SiO quaternary oxide system must be considered for MgO. The various products resulting from dissolution progression were determined by inductively coupled plasma-atomic emission spectrometry (ICP-AES) and X-ray fluorescence (XRF). These results, combined with CSLM analyses, enabled the surface morphology of the particles to be determined. No products formed in M1, M21 or M22. $MgAl_2O_4$ spinel formed in M23 and M24, exhibiting very specific morphology: MgO surrounded by rings of $MgAl_2O_4$ separated by liquid phase, with a different composition to that of the M23 and M24 slags. This observation is illustrated in Fig. 3 and was also made by other authors, not only for MgO inclusions, but also for Al_2O_3 inclusions in slags with MgO [15].

The result for M3 slag was similar to that of slags M23 and M24; however, the ring surrounding the inclusion was identified as another compound, namely Ca_2SiO_4. This also showed retained liquid, but was thicker than in other instances.

Park et al. [2] proposed the following explanation for the formation of the rings. Initially, the compound of the ring is formed on the surface of the inclusion. Since MgO dissolves faster than $MgAl_2O_4$ or Ca_2SiO_4, the latter is dismembered and combines around the inclusion. This is followed by two steps: first, MgO dissolves in the trapped liquid; second, the inner liquid diffuses outwards through $MgAl_2O_4$ or Ca_2SiO_4. These compounds remain at constant thickness due to the dynamic balance established, until MgO replacement is complete. This means that the spinel is no longer being "fed" and, as such, disappears completely. The authors hypothesized that this probably occurs because of spinel's high nucleation rate, while other products nucleate spontaneously around the entire inclusion. Thus, the ring-like structure may occur whenever the slag allows the formation of $MgAl_2O_4$ or Ca_2SiO_4 (crystalline and with high nucleation rates), for both Al_2O_3 and MgO.

5.2.3. *Comments on chemical reactions at the interface*

The studies analyzed show that thermodynamics is subject to physical phenomena resulting from chemical interactions. Among the possible reaction mechanisms, those that deviated most from the predictions of the diagrams were the reactions that prevented direct contact between solid inclusions and liquid slag, that is, when trapped liquid is present [2].

Under these conditions, the system undergoes a complex reaction mechanism that should be avoided since several steps are required for its completion. The result is invariably longer dissolution times for Al_2O_3 inclusions in CaO–SiO_2–Al_2O_3–MgO systems or MgO inclusions in CaO–SiO_2–Al_2O_3 systems. Therefore, the best practice in selecting a slag for inclusion removal is to avoid dissolution pathways that promote the formation of $MgAl_2O_4$ spinel and the calcium silicate Ca_2SiO_4.

5.3. *Influence of the chemical composition of slag*

Cho and Fan [16] reported the results for different slag composition of the CaO–SiO_2–Al_2O_3 system and alumina inclusions. By varying the concentration of silica, alumina and the silica/alumina ratio as well as adding fluxes (CaF_2 and MgO), the authors determined the total time needed for alumina particles measuring $180 \pm 15\,\mu m$ in diameter to dissolve in slag. They found that the dissolution rate of alumina declined with an increase in both the SiO_2 and Al_2O_3 content. Moreover, the addition of up to 4% MgO or CaF_2 increased the alumina dissolution rate even further, with a more pronounced effect for CaF_2 than for MgO.

Taira et al. [17] tested the same system as Cho and Fan [16], but placed liquid slag in contact with an alumina cylinder measuring 17 mm wide by 32 mm high. The authors observed that binary basicity (%CaO/%SiO_2) increased the dissolution speed of alumina. In addition, the increase in dissolution rate in CaO–SiO_2–Al_2O_3 slags is significantly higher when binary basicity is close to 1 (%CaO/%$SiO_2 = 1$). When 15% NaF or CaF_2 was added to this system, for binary basicity between 0.85 and 1.25, the dissolution rate increase two to sixfold in comparison with the same systems when the fluxes are not added.

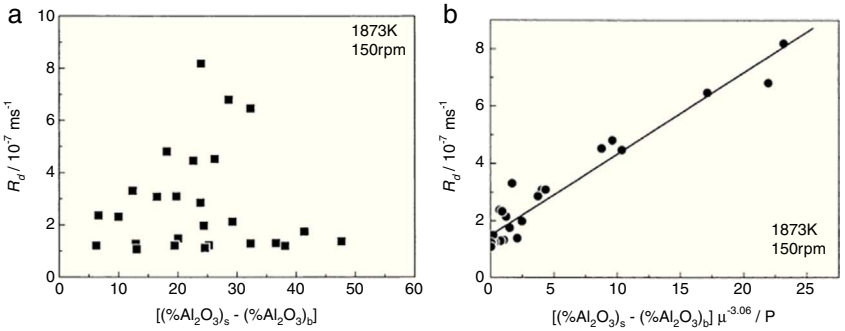

Fig. 4 – Dependence of the alumina dissolution rate for different $CaO–SiO_2–Al_2O_3$ slags as a function of: (a) resulting driving force $[(\%Al_2O_3)_s–(\%Al_2O_3)_b]$ [6]; (b) $[(\%Al_2O_3)_s–(\%Al_2O_3)_b]/\eta^{3.06}$ ratio [6].

However, Choi et al. [6] did not observe such clear relationships when plotting the dissolution rate of alumina versus the driving force (ΔC) for the dissolution reaction in $CaO–SiO_2–Al_2O_3$ slag (Fig. 4(a)).

As such, although the driving force varies with different slag compositions, this approach is not enough to explain why changes in slag composition increase the dissolution rate.

5.4. *Chemical composition, driving force and viscosity*

In an attempt to clarify the relationship between driving force and the dissolution rate of alumina (Fig. 4(a)), Choi et al. [6] used Eq. (1) to plot the dissolution values (dr/dt) as a function of the ratio $[(\%Al_2O_3)_s - (\%Al_2O_3)_b]/\eta^{3.06}$ for different slag compositions in the $CaO–Al_2O_3–SiO_2$ system, obtaining the graph in Fig. 4(b), this time with good linear correlation.

Here, evidence of viscosity (η) is justified, because it significantly affects the contribution of the mass transfer coefficient (k) in Eq. (1).

Valdez, Shannon and Sridhar [3] plotted variables similar to those in Fig. 2.10 and also achieved satisfactory linearity. Next, they devised a formula (Eq. (4)), based on Eq. (2), for a 100 μm aluminum particle.

$$\tau = \frac{2.04 \times 10^{-2}}{\Delta C/\eta} \tag{4}$$

Eq. (4) is of great value due to its similarity to the linear relationship found in Fig. 2.10 and because it demonstrates the proportion of an inclusion's dissolution time (τ) with the driving force (ΔC) and viscosity (η), which are two variables that change considerably depending on the chemical composition selected for the slag.

Valdez et al. [13] report that, in an initial analysis, particle dissolution is controlled by diffusion. Based on this, variations in dissolution rates could be assessed using the differences in driving force and viscosity for different slag-particle systems. Valdez et al. [3] then proposed the diagram in Fig. 5, which shows the composition ranges for $CaO–SiO_2–Al_2O_3$ slags where the driving force to viscosity ratio is more pronounced.

There are four distinct regions in Fig. 5(a). The best alumina dissolution rate will be that for the slag closest to the CaO saturation region. The amount of SiO_2 in this area is minimal.

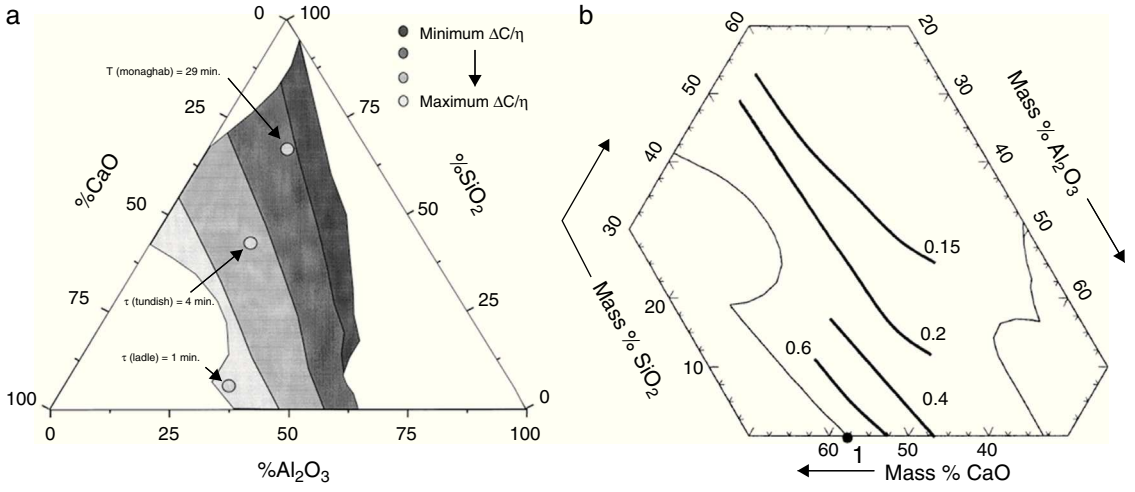

Fig. 5 – (a) Schematic diagram of the influence of slag composition on the $\Delta C/\eta$ ratio for the $CaO–SiO_2–Al_2O_3$ system and 100 μm alumina particles [3]. (b) Ternary diagram showing the lines where the dissolution rate of Al_2O_3 is constant for the $CaO–SiO_2–Al_2O_3$ slag system, with the dissolution rate of reference at point 1 [6].

The mean viscosity (η) is also at its lowest level. Moreover, the highest values for the driving force (ΔC) are also reached in this region. Therefore, the greater the $\Delta C/\eta$, the more efficient is the alumina dissolution [3].

Fig. 5(b) summarizes the study by Choi et al. [6] in the form of a ternary diagram, highlighting the lines representing the constant alumina dissolution rate in the $CaO–Al_2O_3–SiO_2$ system. The result found validates the claims made regarding Fig. 5, since once again higher dissolution rates are observed for liquid compositions closer to CaO saturation.

6. Final comments

Among the influential factors in inclusion absorption by slag, the dependence of saturation on the inclusion/steel contact angle is evident. This hampers the extraction of liquid inclusions, but favors the removal of solid inclusions. On the other hand, data in the available literature show that liquid particles are instantly dissolved on reaching the slag phase, whereas solid particles do not exhibit such intuitive behavior [5,7,11]. Due to its nature, the thermodynamic and kinetic treatment of solid inclusions is essential in predicting dissolution rates. Based on the studies analyzed, it is clear that the formation of compounds at the inclusion/slag interface and high slag viscosity may decrease dissolution capacity. By contrast, this capacity increases when the dissolution pathway does not form kinetically unfavorable compounds or when there is a significant difference in concentration between the interface and the slag. The latter case promotes substantial driving force for dissolution.

Conflicts of interest

The authors declare no conflicts of interest.

Acknowledgements

The support of CNPq, CAPES, FINEP and UFRGS is gratefully acknowledged.

REFERENCES

[1] Jung I, Decterov S, Pelton AD. Computer applications of thermodynamic databases to inclusion engineering. ISIJ Int 2004;44:527–36.

[2] Park JH, Jung IH, Lee HG. Dissolution behavior of Al_2O_3 and MgO inclusions in the $CaO–Al_2O_3–SiO_2$ slags: formation of ring-like structure of $MgAl_2O_4$ and Ca_2SiO_4 around MgO inclusions. ISIJ Int 2006;46:1626–34.

[3] Valdez M, Shannon GS, Sridhar S. The ability of slags to absorb solid oxide inclusions. ISIJ Int 2006;46:450–7.

[4] Yi KW, Tse C, Park JH, Valdez M, Cramb AW, Sridhar S. Determination of dissolution time of Al_2O_3 and MgO inclusions in synthetic $Al_2O_3–CaO–MgO$ slags. Scand J Metall 2003;32:177–87.

[5] AFS INCLUSION ATLAS. Inclusion formation and removal; 2013 http://neon.mems.cmu.edu/afs/afs2/form.html [accessed on February 2013].

[6] Choi JY, Lee HG, Kim JS. Dissolution rate of Al_2O_3 into molten $CaO–SiO_2–Al_2O_3$ slags. ISIJ Int 2002;42:852–60.

[7] Lee SH, Tse C, Yi KW, Misra P, Chevrier V, Orrling C, et al. Separation and dissolution of Al_2O_3 inclusions at slag/metal interfaces. J Non-Cryst Solids 2001;282:41–8.

[8] Choi JY, Lee HG. Wetting of solid Al_2O_3 with molten $CaO–Al_2O_3–SiO_2$. ISIJ Int 2003;43:1348–55.

[9] Fruehan RJ. The making shaping and treating of steel – steelmaking and refining. 11th ed. Pittsburgh, PA: AISE Steel Foundation; 1998.

[10] Daoud ILA (Dissertação (Mestrado em Engenharia)) Estudo numérico do escoamento e do comportamento de inclusões não-metálicas em distribuidores de lingotamento contínuo de aço. Porto Alegre: Escola de Engenharia, Programa de Pós-Graduação em Engenharia de Minas, Metalúrgica e Materiais da UFRGS; 2006. p. 116.

[11] Millman S. Clean steel – basic features and operation practices. In: IISI study on clean steel, IISI committee on technology. 2004. p. 39–60.

[12] Bouris D, Bergeles G. Investigation of inclusion re-entrainment from the steel–slag interface. Metall Mater Trans B 1998;29B:641–9.

[13] Valdez M, Prapakorn K, Sridhar S, Cramb AW. Dissolution of inclusions in steelmaking slags. In: ISSTech 2003 conference proceedings. 2003.

[14] Levenspiel O. Chemical reaction engineering. 3rd ed. New York: John Wiley & Sons; 1999.

[15] Valdez M, Prapakorn K, Cramb AW, Sridhar S. Dissolution of alumina particles in $CaO–SiO_2–Al_2O_3–MgO$ slags. Ironmak Steelmak 2002;29:47–52.

[16] Cho WD, Fan P. Diffusional dissolution of alumina in various steelmaking slags. ISIJ Int 2004;44:229–34.

[17] Taira S, Nakashima K, Mori K. Kinetic behavior of dissolution of sintered alumina into $CaO–SiO_2–Al_2O_3$ slags. ISIJ Int 1993;33:116–23.